physica **pssb** status solidi

www.pss-b.com

basic solid state physics

Joint Raman spectroscopy and HRXRD investigation of cubic gallium nitride layers grown on 3C-SiC

M. Rüsing*, T. Wecker, G. Berth, D. J. As, and A. Zrenner

Department Physik, Universität Paderborn, Warburger Strasse 100, 33098 Paderborn, Germany

* Corresponding author: e-mail michael.ruesing@upb.de, Phone: +49-5251-60-5805, Fax: +49-5251-60-3710

Cubic gallium nitride (GaN) films are analyzed with high-resolution X-ray diffraction (HRXRD) and Raman spectroscopy. Several cubic GaN layers were grown on 3C-SiC (001) substrate by radio-frequency plasma-assisted molecular beam epitaxy. The layer thickness of the cubic GaN was varied between 75 and 505 nm. The HRXRD analysis reveals a reduction of the full-width at half-maximum (FWHM) of omega scans for growing layer thicknesses, which is caused by a partial compensation of defects. The Raman characterization con-

firms well-formed c-GaN layers. A more detailed examination of the longitudinal optical mode hints at a correlation of the FWHM of the Raman mode with the dislocation density, which shows the possibility to determine dislocation densities by Raman spectroscopy on a micrometer scale, which is not possible by HRXRD. Furthermore, this Raman analysis shows that normalized Raman spectra present an alternative way to determine layer thicknesses of thin GaN films.

1 Introduction In recent years, the interest in the material class of group III-nitrides has strongly increased, especially in the fields of THz devices and fast modulators and photo detectors [1]. The huge band offset of GaN/AlN heterostructures enables a wide adjustment of intraband transitions needed for devices operating around the 1.55 μm spectral region (optical C-band) [2]. Strong internal polarization fields along the *c*-axis in hexagonal group III nitrides complicate the design of complex devices based on low-dimensional structures severely [3]. These internal fields lead to bending of the bands and the quantum-confined Stark-effect. Another consequence is the spatial separation of electron and hole wave functions, thus the efficiency of such devices is strongly reduced. One solution mainly used for this problem in the hexagonal phase is the growth of semi-polar group III nitrides on substrates with different directions [4]. Due to the high symmetry cubic GaN/AlN contains no internal polarization fields along the growth axis. Hence, devices based on low-dimensional structures containing the cubic phase grown on 3C-SiC in (001) direction can be exploited much more easier.

Raman spectroscopy (RS) is a widely employed technique to study the vibrational properties of solid state systems

[5, 6]. Due to the strong connection of the vibrational properties to changes in the crystal structure, RS can be utilized to characterize numerous material properties, such as crystal structure, symmetry and different phases [7, 8], defects [9], or dielectric constants [10]. Detailed analysis of the spectral line shapes also allows for characterization of phonon confinement and (nano-)particle sizes [11, 12] or the determination of free carrier densities [13–15]. In confocal application, RS may even be used to resolve the spatial distribution of certain properties, such as strain [16] or anti-phase domains [17]. One of the main advantages of RS is the noninvasive character and usually it does not require special sample treatment. So, it is one of the foremost methods to study semiconductor systems.

The electrical and optical performance of semiconductor devices are heavily limited by defects. Therefore, the characterization and determination of defect types and defect densities are key requirements for growth process optimization. Previous studies have established that the predominant extended defect type in cubic GaN (c-GaN) are stacking faults (SFs) along (111) planes [18–22]. Here, the number of defects is directly correlated to the substrate smoothness [23]. The geometry of these SFs allows for an annihilation process.

Wiley Online Library

Phys. Status Solidi B 253, No. 4 (2016)

Original

Paper

779

Table 1 Summary of determined sample properties including layer thickness d, omega scan FWHM $\Delta\theta$, the determined defect density D, and the Raman FWHM of the c-GaN LO peak $\Delta\bar{\nu}$.

d (nm)	$\Delta\theta$ (arc min)	D (10^9 cm^2)	$\Delta\bar{\nu}$ (cm^{-1})
505	32.4	9.73	11.2
460	31.3	9.06	10.8
475	32.9	10.0	11.1
380	35.4	11.6	10.7
150	42.6	16.8	12.9
75	49.2	22.4	13.4

If two SFs, oriented along (111) and (11$\bar{1}$), for example, intersect they annihilate leaving a sessile dislocation [24, 25]. This directly leads to an increase of crystal quality for thicker layers [23].

In previous work, this behavior and defect have been studied extensively with high-resolution X-ray diffraction (HRXRD) and transmission electron microscopy (TEM). So far to our knowledge, no study was performed on the sensitivity of RS on the effect. Therefore, in this work a series of cubic GaN samples on 3C-SiC substrate of various thickness have been grown. The samples are characterized in a joint investigation of HRXRD and RS.

2 Experimental details Thick cubic GaN (001) layers were grown on a 10 µm 3C-SiC (001) layer deposited on a 0.5 mm thick Si substrate. The layer thickness was varied from 75 to 505 nm. For the growth, a Riber-32 radio-frequency plasma-assisted molecular beam epitaxy (PAMBE) system was used equipped with standard effusion cells for Ga and Al evaporation. Atomic nitrogen is provided by an Oxford plasma source and the growth process can be controlled *in situ* by Reflection High Energy Electron Diffraction (RHEED). The growth of c-GaN was realized at a substrate temperature of $T_S = 720°C$ with one monolayer of Ga excess on the sample surface. More details concerning the growth of cubic GaN on 3C-SiC can be found in Ref. [26]. Atomic force microscopy measurements revealed an RMS surface roughness of around 5 nm for 5×5 µm^2 areas. The obtained sample thickness was verified with Reflectometric Interference Spectroscopy [27]. Here, our system achieves a resolution in the range of ±25 nm . The most important parameters of the samples are summarized in Table 1.

For characterization of the c-GaN layer, quality HRXRD scans and reciprocal space maps (RSM) have been taken with a Philips X'Pert materials research diffractometer with a copper anode. The Raman experiment was performed on a custom-built µ-Raman setup in back-scattering geometry. The excitation light was provided by a frequency-doubled Nd:YAG at 532 nm with an output power of about 50 mW. The light was focused to a spot with a diameter of less than 1 µm. The scattered light was analyzed in a spectrometer with integrated Notch-filter and holographic-grating (KOSI Holospec f/1.8i) and an attached CCD camera for data acquisition (Andor Newton, BI). The system reaches a spectral
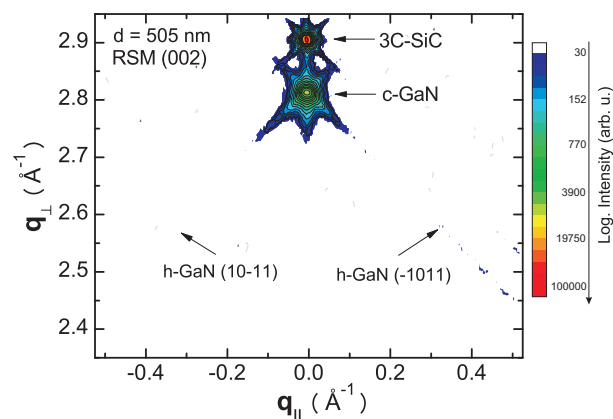
Figure 1 Reciprocal space map (RSM) around the (002) diffraction peak of the c-GaN for $d = 505$ nm sample. The RSM shows almost no signal of hexagonal inclusions. Comparing the intensity of the c-GaN and h-GaN peaks yields hexagonal inclusions of less than 1%.

resolution of approximately 2.3 cm^{-1}. Further details about the experimental setup may be taken from Refs. [28, 29].

3 Results and discussion

3.1 Structural properties To characterize the structural properties and defect densities of the sample, HRXRD and RSM measurements have been performed. A typical RSM taken from the 505 nm sample is shown in Fig. 1. The (002) reflex of c-GaN and 3C-SiC is clearly visible. The position, where the (10$\bar{1}$1) and ($\bar{1}$011) reflexes of h-GaN are expected, is highlighted in the graph. Here, only a very weak signal related to h-GaN just above noise level is detected even in the thickest sample. The intensity ratios of the c-GaN and h-GaN can be used to estimate the percentage of the hexagonal inclusion [30]. This calculations yield hexagonal inclusions of less than 1% for all of our samples. The defect densities are calculated from the FWHM $\Delta\theta$ of an ω-scan of the (002) diffraction peak based on the method by Gay [31]. The dislocation density D is then given by

$$D = \frac{\Delta\theta^2}{9b^2}, \tag{1}$$

with b, the length of the Burgers vector. The Burgers vector for a dislocation in a cubic zinc-blende crystal, such as c-GaN, is given by $b = a/\sqrt{2}$, where a is the lattice parameter [32]. The lattice constant for c-GaN is taken to be $a = 4.503$ Å [33, 34]. The calculated values for the dislocation densities are summarized in Table 1. As expected, the defect density decreases with growing layer thickness. The observed values span from 9×10^9 cm^2 to 2×10^{10} cm^2, which is in the typical range of 10^9 cm^2 to 10^{10} cm^2 previously reported for c-GaN grown on 3C-SiC substrate [20, 23, 25]. For thicknesses in the range of 400–500 nm, no significant improvement of the full-width at half-maximum in Raman and HRXRD can be observed anymore. A possible explanation is the SFs have mostly annihilated and other defects become predominant in this thickness range.
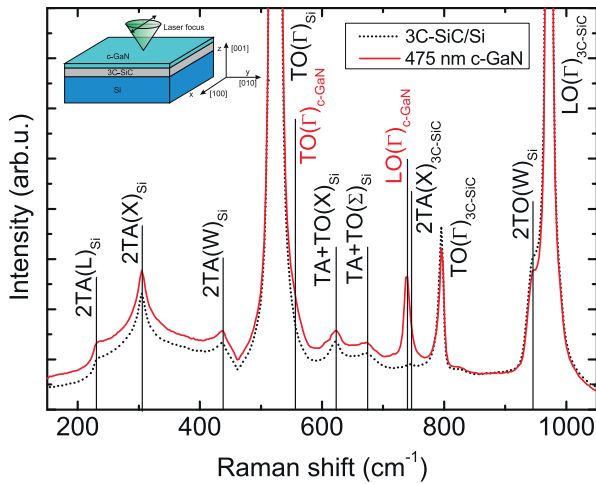
Figure 2 Typical back-scattering Raman spectra of a c-GaN layer on 3C-SiC substrate (dotted) compared to substrate material (full line). Two features can unambiguously be attributed to c-GaN (highlighted in red). Other features in the spectrum are related to one- and two-phonon scattering in Si and 3C-SiC originating from various points in the Brillouin zone (see text). The inset shows the measurement geometry.

3.2 μ-Raman spectroscopy

Figure 2 shows a typical back-scattering Raman spectrum of c-GaN on 3C-SiC/Si substrate. The sample structure and geometry are shown in the inset. For comparison, a spectrum of the unprocessed substrate is added. Some distinct features in the spectrum have been labeled according to the related process. The spectra are largely dominated by the peak of the zone-center transversal optical (TO) phonon of silicon at about $521\,cm^{-1}$ and the zone-center TO and longitudinal optical (LO) phonon of the 3C-SiC detected at 795 and $972\,cm^{-1}$, respectively. Most other features are related to two-phonon overtone scattering in the Si and 3C-SiC substrate. The spectral shape largely resembles the phonon density of states in the respective material [35–39]. Here, for example, the feature at $306\,cm^{-1}$ labeled with $2TA(X)_{Si}$ is an overtone of a transverse acoustical (TA) mode in silicon (Si) originating from the X-point in k-space, while $TA + TO(X)_{Si}$ is a TA and TO combination band at the X-point.

By comparing the spectra, two characteristics can unambiguously be attributed to c-GaN. In the spectra, the most distinct difference is a band at $738\,cm^{-1}$, which is attributed to the zone-center LO mode of c-GaN. The measured Raman shift agrees well with the literature data [7, 9, 40]. The corresponding TO mode is only barely visible as a shoulder at approximately $550\,cm^{-1}$, but it is much weaker in intensity, because of Raman selection rules for cubic materials. Here, zone-center TO scattering is forbidden from cubic (001) surfaces in back-scattering geometry. But it is still weakly detectable, because of activation by defects and contributions by forward scattering by multiple reflections [13, 41]. The same effect can also be observed for the LO and TO modes of the 3C-SiC, which is of the same crystal symmetry. Here, the TO signal is significantly weaker in comparison to the

LO (Fig. 2). The c-GaN TO cannot be identified in the 75 and 150 nm sample. It becomes undetectable for layer thicknesses between 150 and 380 nm. Therefore, no conclusive analysis of the c-GaN TO was possible and further analysis will be limited to the c-GaN LO. In addition, no peaks related to the hexagonal phase of GaN could be detected. Here, even small inclusions of hexagonal phase will lead to a strong peak at $560–570\,cm^{-1}$ related to the E_2^H and E_1-TO modes of h-GaN [9, 42], which have not been detected in any of our samples. This confirms the high-quality cubic crystal structure in agreement to the HRXRD analysis.

For better comparability, the spectra have been normalized with respect to the silicon zone-center TO peak. For the normalization, it is assumed that the scattering in the thin c-GaN layers is weak compared to the total intensity. The c-GaN LO peak has been fitted with a Lorentzian of the form

$$I(\bar{\nu}) = \frac{A}{2\pi} \frac{\Delta\bar{\nu}}{(\omega - \omega_0)^2 + (\Delta\bar{\nu}/2)^2}, \tag{2}$$

the integrated peak area is A, ω_0 the peak central wavenumber, and $\Delta\bar{\nu}$ the FWHM of the peak. To improve the fitting results, the spectrum of the c-GaN has been corrected for the substrate signal. In particular, this improved the fitting results for the thinner layers, because an acoustical phonon overtone of 3C-SiC at $745\,cm^{-1}$ leads to a considerable asymmetry in the c-GaN LO peak shape. The LO in all spectra could be fitted very well with a Lorentzian. It should be noted for neither sample an asymmetry or shift to higher wave numbers in the LO could be detected, which otherwise would have indicated free charge carriers in the system [9, 13]. The values for the FWHM $\Delta\bar{\nu}$ are summarized in Table 1. The correction of the FWHM due to finite slit width [43, 44] has been omitted, because in this study the main focus lies on the comparison of the relative changes in the FWHM.

The intensity of the detected Raman signal depends on the number of scattering centers, which is given by the scattering volume V, and the intensity distribution $I(x, y, z)$ of the excitation light. Therefore, the observed intensity of a given Raman band is proportional to

$$\int_V I(x, y, z)\mathrm{d}V.$$

The intensity distribution of light focused through an objective lens is given by the Point Spread function (PSF). After Ref. [45], the PSF is given by

$$I(x, y, z) = (2/u)^2 \left[U_1^2(u, v) + U_2^2(u, v) \right], \tag{3}$$

where U_1 and U_2 are Lommel functions and the variables u and v are given by $u = 2\pi NA z/\lambda$ and $v = 2\pi NA \sqrt{x^2 + y^2}/\lambda$. We have assumed the PSF center ($z = 0\,\mu m$) inside the c-GaN film and have evaluated Eq. (3) within $x, y = \pm 10\,\mu m$ and $z = \pm d/2$ for our objective lens with a numerical aperture $NA = 0.7$. The result is depicted

Phys. Status Solidi B 253, No. 4 (2016)

781
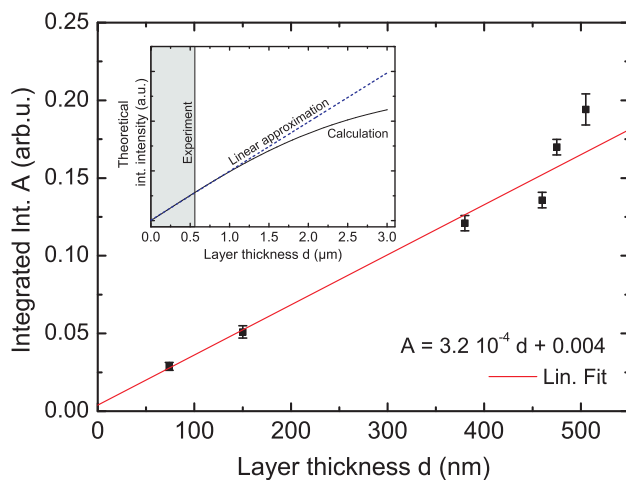
Figure 3 The inset shows the integral value of the Point Spread Function (PSF) calculated in the limits of $\pm d/2$ around the maximum of the PSF. For values $d < 1\,\mu$m, the integrated intensity grows almost linearly. In agreement with this model, our measured integrated peak areas A of the normalized c-GaN LO peaks suggest a linear behavior with respect to the thickness d.

Figure 4 Dislocation density D as determined by the HRXRD analysis versus the FWHM of the c-GaN LO peak $\Delta\bar{\nu}$. The data points are labeled according to the sample thickness. The data indicate a correlation in the studied thickness range, which suggest that Raman spectroscopy data may be directly used to study dislocation densities. The dashed line is meant as a guide to the eye.

in the inset in Fig. 3 and shows an almost linear growth of the integrated intensity for $d < 1\,\mu$m, which includes the regime of our experiment.

Figure 3 shows the integrated intensity A obtained from the fits with respect to the layer thickness. Here, the data show a good agreement with the anticipated linear behavior. The fitted graph intersects the point of origin within the confidence value of the fitting results. Hence, RS presents a completely different approach to calculate the layer thicknesses d and provides even accurate results for fairly thin layers (< 100 nm), which usually are difficult to measure with Reflectometric interference spectroscopy.

The FWHM of Raman bands is often used as a benchmark for determining the quality and homogeneity of crystalline systems. Table 1 compares the determined values of the LO FWHM with the HRXRD data. The data suggest a correlation between both values. Therefore, Raman FWHM data may be directly used to determine dislocation densities. Figure 4 shows the Raman FWHM $\Delta\bar{\nu}$ plotted with respect to the determined dislocation density. The data hint at a clear correlation between the dislocation density and the Raman FWHM of the LO. The LO FWHM clearly increases for higher dislocation densities, which is also indicated by the dashed line. The four thickest samples show nearly the same value for the FWHM. On the one hand, this is connected to the fact that these samples also show nearly the same value for the dislocation density as determined by HRXRD. Hence, only small differences in the FWHM can be expected. On the other hand, this might be due to the fact that the limit of the homogeneous line width is reached and the dislocation density is not the dominant effect in the LO FWHM anymore. Further studies are necessary to investigate the functional relation and the limits of the correlation. Nevertheless, it can

be concluded that μ-Raman spectroscopy presents a way to study dislocation densities even on a micrometer scale and therefore offers a much better resolution than HRXRD.

4 Conclusions Cubic GaN layers of various thicknesses have been grown with PAMBE on (001) 3C-SiC substrate. The thickness was varied between 75 and 505 nm. Raman Spectroscopy was compared with the usually exploited HRXRD measurements to investigate the structural quality of these samples. Both methods confirm phase pure c-GaN with no measurable hexagonal inclusions. Applying the model of Gay, the dislocation density was calculated from the FWHM of the HRXRD (002) diffraction peak. Here, a decrease in dislocation density with growing layer thicknesses was found in accordance to the literature. This decrease could also be observed in the Raman data, which suggests a direct correlation between the FWHM $\Delta\bar{\nu}$ of the Raman LO band and the HRXRD data for the analyzed samples. Further, appropriately normalized Raman spectra can directly be used to determine the layer thickness of the grown films via the intensity of the c-GaN peaks. The analysis suggests that this technique may even work accurately for thin layers in the sub 100 nm range. Overall, Raman spectroscopy enables a direct and fast evaluation of dislocation densities and layer thicknesses without the need for any special sample preparation.

References

[1] H. Machhadani, M. Tchernycheva, S. Sakr, L. Rigutti, R. Colombelli, E. Warde, C. Mietze, D. J. As, and F. H. Julien, Phys. Rev. B **83**, 075313 (2011).

[2] C. Gmachl and H. M. Ng, Electron. Lett. **39**(6), 567–569 (2003).

[3] M. Beeler, C. Bourgerol, E. Bellet-Amalaric, and E. Monroy, Phys. Status Solidi A **211**(4), 761–764 (2014).

[4] F. Scholz, Semicond. Sci. Technol. **27**, 024002 (2012).

[5] P. Y. Yu and M. Cardona, Fundamentals of Semiconductors, 3rd edition (Springer, Berlin, Heidelberg, New York, 2005).

[6] D. Gardiner, H. Bowley, P. Graves, D. Gerrard, J. Louden, and G. Turrell, Practical Raman Spectroscopy (Springer, Berlin, Heidelberg, 2012).

[7] T. Frey, D. J. As, M. Bartels, A. Pawlis, K. Lischka, A. Tabata, J. R. L. Fernandez, M. T. O. Silva, J. R. Leite, C. Haug, and R. Brenn, J. Appl. Phys. **89**, 2631 (2001).

[8] H. Morkoc, Handbook of Nitiride Semiconductors and Devices (Wiley-VCH, Weinheim, 2008).

[9] H. Harima, J. Phys.: Condens. Matter **14**, R967–R993 (2002).

[10] R. H. Lyddane, R. G. Sachs, and E. Teller, Phys. Rev. **59**, 673–676 (1941).

[11] H. Richter, Z. P. Wang, and L. Ley, Solid State Commun. **39**, 625–629 (1981).

[12] A. K. Arora, M. Rajalakshmi, T. R. Ravindran, and V. Sivasubramanian, J. Raman Spectrosc. **38**, 604–617 (2007).

[13] Y. A. Pusep, M. T. O. Silva, J. R. L. Fernandez, V. A. Chitta, J. R. Leite, T. Frey, D. J. As, D. Schikora, and K. Lischka, J. Appl. Phys. **91**, 6197 (2002).

[14] T. Kozawa, T. Kachi, H. Kano, Y. Taga, M. Hashimoto, N. Koide, and K. Manabe, J. Appl. Phys. **75**, 1098 (1994).

[15] H. Harima, S. Nakashima, and T. Uemura, J. Appl. Phys. **78**, 1996 (1995).

[16] M. Panfilova, A. Pawlis, C. Arens, S. Michaelis de Vasconcellos, G. Berth, K. P. Hüsch, V. Wiedemeier, A. Zrenner, and K. Lischka, Microelectron. J. **40**, 221–223 (2009).

[17] R. M. Kemper, T. Schupp, M. Häberlen, T. Niendorf, H. J. Maier, A. Dempewolf, F. Bertram, J. Christen, R. Kirste, A. Hoffmann, J. K. N. Lindner, and D. J. As, J. Appl. Phys. **110**, 123512 (2011).

[18] E. Martinez-Guerrero, E. Bellet-Amalric, L. Martinet, G. Feuillet, B. Daudin, H. Mariette, P. Holliger, C. Dubois, C. Bru-Chevallier, P. Aboughe Nze, T. Chassagne, G. Ferro, and Y. Montei, J. Appl. Phys. **91**, 4983 (2002).

[19] A. Trampert, O. Brandt, H. Yang, and K. H. Ploog, Appl. Phys. Lett. **70**, 583 (1997).

[20] H. Okumura, K. Ohta, G. Feuillet, K. Balakrishnan, S. Chichibu, H. Hamaguchi, P. Hacke, and S. Yoshida, J. Cryst. Growth **178**, 113–133 (1997).

[21] D. Wang, Y. Hiroyama, M. Tamura, M. Ichikawa, and S. Yoshida, J. Cryst. Growth **220**, 204–208 (2000).

[22] H. Yang, O. Brandt, and K. Ploog, J. Electron. Mater. **25**(5), 787 (1996).

[23] B. Daudin, G. Feuillet, J. Hbner, Y. Samson, F. Widmann, A. Philippe, C. Bru-Chevallier, G. Guillot, E. Bustarret, G. Bentoumi, and A. Deneuville, J. Appl. Phys. **84**, 2295 (1998).

[24] H. Yang, L. X. Zheng, J. B. Li, X. J. Wang, D. P. Xu, Y. T. Wang, X. W. Hu, and P. D. Han, Appl. Phys. Lett. **74**, 2498 (1999).

[25] D. J. As, Proc. SPIE **7608**, 76080G (2010).

[26] J. Schörmann, S. Potthast, D. J. As, and K. Lischka, Appl. Phys. Lett. **90**, 041918 (2007).

[27] C. Hänel and G. Gauglitz, Anal. Bioanal. Chem. **372**, 91–100 (2002).

[28] V. Wiedemeier, G. Berth, A. Zrenner, E. M. Larramendi, U. Woggon, K. Lischka, and D. Schikora, Semicond. Sci. Technol. **26**, 105023 (2011).

[29] G. Berth, W. Hahn, V. Wiedemeier, A. Zrenner, S. Sanna, and W. G. Schmidt, Ferroelectrics **420**(1), 44–48 (2011).

[30] X. L. Sun, Y. T. Wang, H. Yang, J. B. Li, L. X. Zheng, D. P. Xu, and Z. G. Wang, Thin Solid Films **368**, 237–240 (2000).

[31] P. Gay, P. B. Hirsch, and A. Kelley, Acta Metall. **1**, 315 (1953).

[32] D. Hull and D. Bacon, Introduction to Dislocation (Butterworth-Heinemann, Oxford, 2011).

[33] T. Wecker, F. Hörich, M. Feneberg, R. Goldhahn, D. Reuter, and D. J. As, Phys. Status Solidi B **252**(5), 873–878 (2015).

[34] K. Kim, W. R. L. Lambrecht, and B. Segall, Phys. Rev. B **52**(24), 16310–16326 (1996).

[35] K. Uchinokura, T. Sekine, and E. Matsuura, J. Phys. Chem. Solids **35**, 171–180 (1974).

[36] P. A. Temple and C. E. Hathaway, Phys. Rev. B **7**(8), 3685–3697 (1973).

[37] P. Giannozzi, S. de Gironcoli, P. Pavone, and S. Baroni, Phys. Rev. B **43**(9), 7231–7242 (1991).

[38] K. Karch, P. Pavone, W. Windl, O. Schütt, and D. Strauch, Phys. Rev. B **50**(23), 17054–17063 (1994).

[39] D. W. Feldman, J. H. Parker, Jr., W. J. Choyke, and L. Patrick, Phys. Rev. **173**(3), 787–793 (1968).

[40] H. Harima, T. Inoue, S. Nakashima, H. Okumura, Y. Ishida, S. Yoshida, T. Koizumi, H. Grille, and F. Bechstedt, Appl. Phys. Lett. **74**, 191 (1999).

[41] M. Giehler, M. Ramsteiner, O. Brandt, H. Yang, and K. H. Ploog, Appl. Phys. Lett. **67**, 733 (1995).

[42] H. Siegle, L. Eckey, A. Hoffmann, C. Thomsen, B. Meyer, D. Schikora, M. Hankeln, and K. Lischka, Solid State Commun. **96**(12), 943–949 (1995).

[43] F. G. Dijkman and J. H. V. D. Maas, Appl. Spectrosc. **30**(5) (1976).

[44] K. Tanabe and J. Hiraishi, Spectrochim. Acta **36A**, 341–344 (1980).

[45] M. Born and E. Wolf, Principles of Optics: Electromagnetic Theory of Propagation, Interference and Diffraction of Light, 7th edition (Cambridge University Press, Cambridge, 1999).